Available online at www.sciencedirect.com

SciVerse ScienceDirect

Ceramics International 38 (2012) 3069–3074

CERAMICS INTERNATIONAL

www.elsevier.com/locate/ceramint

Effect of particle size distribution of alumina on strength of glass-infiltrated alumina

Hyung Bong Lim, Won-Seung Cho, Cheol Y. Kim *

Department of Materials Science and Engineering, INHA University, Incheon, Republic of Korea

Received 19 September 2011; received in revised form 30 November 2011; accepted 2 December 2011
Available online 9 December 2011

Abstract

Glass-infiltrated alumina composites were prepared by infiltrating glass into a pre-sintered alumina. Three different alumina preforms were obtained from various combinations of fine and coarse alumina particles. After infiltration of glass into the porous alumina preforms, their microstructure and strength were studied. The highest bending strength of 510 MPa was observed when the composite was made by mixing coarse and fine alumina powders at a ratio of 6:4. The infiltrated glass corroded the alumina preform, and the dissolved aluminum ions reprecipitated on the alumina grains during the heat-treatment for infiltration.

Keywords: C. Strength; Alumina; Glass infiltration; Microstructure

1. Introduction

The technique of infiltrating a molten salt into a porous ceramics has been successfully applied to the manufacture of ceramic filters, membranes and artificial teeth [1]. For artificial teeth, such as coping, in-lay, on-lay and veneer, the infiltration is carried out with molten glasses which have a transparent property in order to achieve aesthetics like a natural tooth [1,2]. Another merit of glass-infiltrated ceramic composites for dental applications is that they have excellent, accurate fitting after heat-treatment [3] because the glass melt infiltrates into porous media without shrinkage of the composites.

A porous medium, or ‘‘preform’’, could be prepared with spinel, zirconia or alumina ceramics [4]. Among these, alumina preforms provide the most accurate fit for the final product, because less shrinkage is incurred in the alumina than in the other materials during infiltration [5]. The major drawback of alumina is, however, its low strength in applications such as bridges and molar teeth, which present high mastication pressure. Lee et al. [6] reported that alumina particle size and distribution influenced the mechanical properties of glass-infiltrated alumina composites. However, the mechanical properties of grain growth with infiltration temperature were not studied. Lee and Kim [7] reported that the high strength of the glass-infiltrated alumina composite comes from the deflected crack propagation around the alumina particles. However, the correlation between strength and alumina particle size has not been identified.

The primary objective of this study is, therefore, to examine the effect of alumina particle size as a function of infiltration temperature on the microstructure and the strength of the glass-infiltrated alumina composite.

2. Experimental procedure

Four different alumina preforms were prepared with alumina powders that had different particle sizes and distributions. Coarse powder with an average size of 4.75 μm was obtained as purchased (A1100 series, 98.5 purity, Spectrum Chemical MFG Co., USA) and fine power with an average size of 0.27 μm was obtained by pulverizing the coarse powder in a planetary mill for 24 h. Four different alumina batches were prepared by mixing the coarse and fine alumina powders at ratios of 10:0 (C1.0), 6:4 (C0.6), 4:6 (C0.4) and 0:10 (C0.0). Cylindrical alumina preforms with a diameter of 20.0 mm and height of 2.0 mm were formed by a slip-casting method; these preforms were sintered at 1170 °C for 1 h to develop a porous structure for the glass infiltration without shrinkage of a skeleton during sintering.

* Corresponding author.
E-mail address: cheolkim@inha.ac.kr (C.Y. Kim).

0272-8842/$36.00
doi:10.1016/j.ceramint.2011.12.005

The glass composition for the infiltration was $31SiO_2$–$23B_2O_3$–$17Al_2O_3$–$5CaO$–$13La_2O_3$–$7TiO_2$–$3CeO_2$–$0.68Fe_2O_3$ (in mol%). The glass batch was prepared by mixing first grade chemicals; the batch was then melted in a Pt crucible at 1500 °C for 2 h. The glass melt was poured on a graphite plate and the glass disk was crushed into small particles. Disk was then re-melted in a platinum crucible under the previous melting conditions for improved glass homogeneity. The molten glass was quenched in water and pulverized into a fine powder with a size of 80–120 μm. The glass powder was suspended in distilled water, and the slurry was placed on the pre-sintered alumina preform before heat-treatment at 1150 °C or 1300 °C for various times from 1 min to 12 h for the infiltration. After infiltration, excess glass was removed with a diamond grinder and sand blaster machine. The specimens were annealed at 850 °C for 10 min in order to remove any possible residual stress.

The alumina particle distribution was determined with a laser particle size analyzer (Mastersizer 2000, Malvern Instruments Ltd., UK) and the density of the alumina preform was measured with the Archimedes method. The pore size and distribution were investigated by Hg porosimeter (Poresizer 9320, Micromeritics). The microstructure of the composites was examined by scanning electron microscopy (SEM, JEOL) after etching in 50 vol% HF solution for 30 s. The strength of the specimens before and after the glass infiltration was evaluated with a flat-on-three-ball biaxial flexure testing system at a stress rate of 23 MPa s^{-1}.

3. Results and discussion

3.1. Densification and biaxial strength of glass-infiltrated alumina

Fig. 1 shows the alumina particle size distribution for each batch, and Fig. 2 shows the pore size distribution for each alumina preform after it was pre-sintered at 1170 °C for 1 h. Table 1 summarizes the median alumina particle diameters,

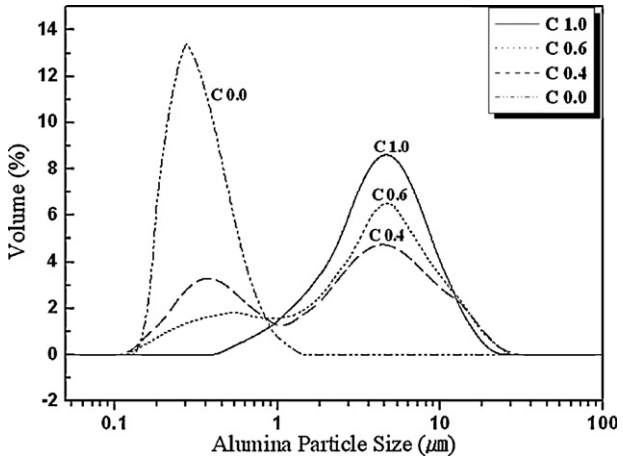

Fig. 1. Particle size distribution of alumina powders for each alumina preform batch.

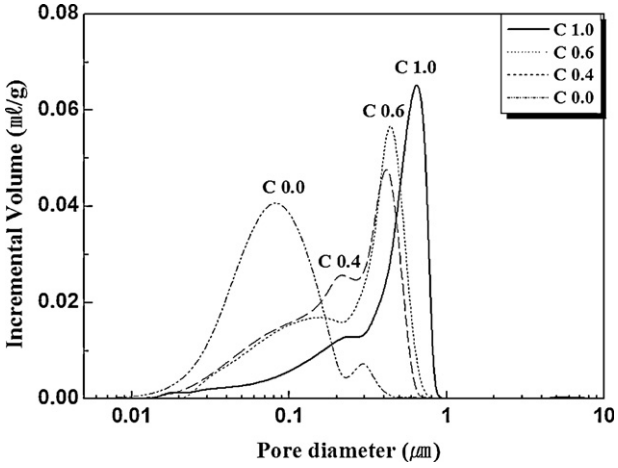

Fig. 2. Pore size distribution for each alumina preform.

pore diameters and porosities for each sample, which are obtained from Figs. 1 and 2.

Alumina batches of samples C1.0 and C0.0 show a unimodal particle distribution, while alumina batches of samples C0.6 and C0.4 show a broad and bimodal particle distribution because they are mixtures of coarse and fine powders. The pore diameter and porosity of the pre-sintered preforms decreased with the addition of fine alumina powder to the coarse one, as shown in Table 1. This indicates that the fine alumina particles fill the interstices among the coarse alumina particles. It is conceivable that the size and distribution of these alumina particles are closely related to the microstructure and strength of the alumina composite infiltrated by glass.

The glass was infiltrated into an alumina preform that was pre-sintered at 1170 °C for 1 h; the densifications of the glass-infiltrated alumina composite are given in Fig. 3. The densification is assessed by the decrease in porosity of the composite before and after glass infiltration according to the equation below [8].

$$\Psi(\%) = \frac{(P_1 - P_2)}{P_1} \times 100$$

where Ψ is the densification of the composite, and P_1 and P_2 are the porosity of the preform before and after infiltration, respectively.

When the glass was infiltrated at 1150 °C for 80 min (Fig. 3(a)), sample C1.0 reached 95% of the densification, but the sample C0.0 reached only 80% of the densification. Because sample C1.0 has larger pores, it is easy for the glass

Table 1
Median values of particle diameter, porosity and pore diameter for the pre-sintered alumina preforms.

Samples	Alumina preform		
	Particle diameter (μm)	Porosity (%)	Pore diameter (μm)
C1.0	4.75	53.5	0.47
C0.6	4.31	42.9	0.36
C0.4	3.73	40.1	0.22
C0.0	0.27	37.9	0.10

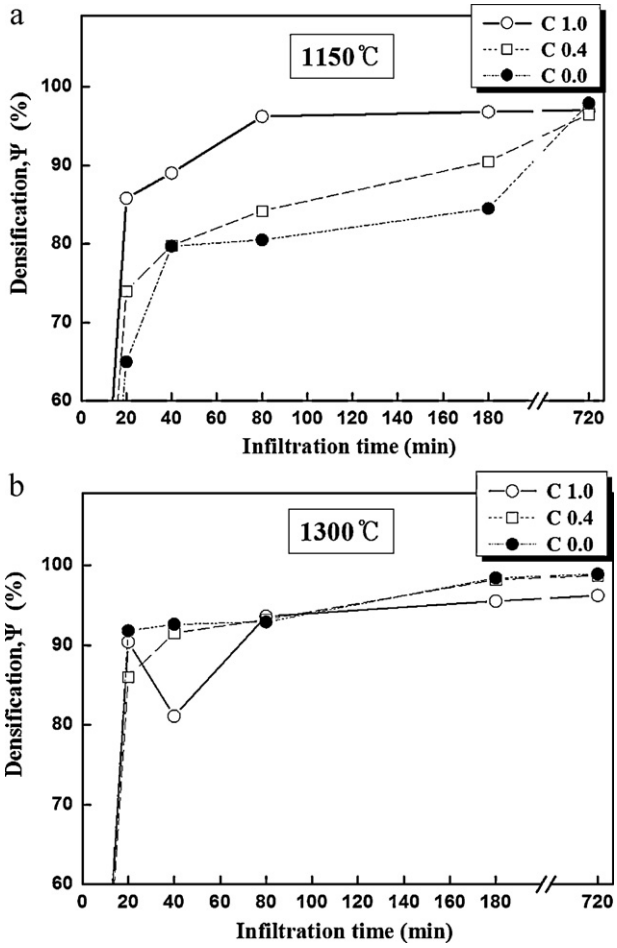

Fig. 3. Densification of glass-infiltrated alumina composites after infiltration at (a) 1150 °C and (b) 1300 °C for various times.

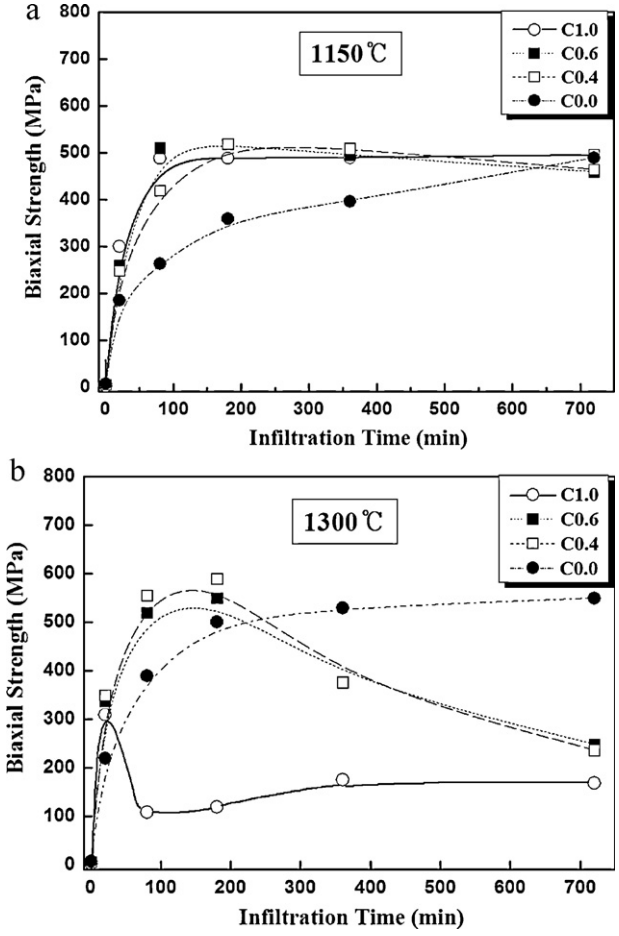

Fig. 4. Biaxial strength of glass-infiltrated alumina composites after infiltration at (a) 1150 °C and (b) 1300 °C for various times.

melt to flow down to the pores. This promotes the densification at the early stages of infiltration.

When the glass was infiltrated at 1300 °C (Fig. 3(b)), however, a rapid initial densification was observed within 20 min of the infiltration for samples C0.0 and C0.4, regardless of the pore size, because the viscosity of the glass melt at 1300 °C is expected to be much lower than that at 1150 °C. A sharp decrease in the densification for sample C1.0 was observed after 20 min of infiltration. This could be attributed to the swelling phenomena of the sample before the rearrangement of the alumina particles, and due to the rapid glass infiltration into the macro pores.

The biaxial strengths for the glass-infiltrated alumina after the infiltration at 1150 °C or 1300 °C for various times are shown in Fig. 4. When the glass was infiltrated at 1150 °C (Fig. 4(a)), the biaxial strength for specimens C1.0, C0.6 and C0.4 sharply increased to about 500 MPa with the filling of the pores with glass; the strength is nearly constant after 180 min of infiltration time, suggesting that the filling of the pores by glass was completed by this time. However, the strength of the sample C0.0 increased rather slowly because this sample has smaller pores and needs some time to complete the glass infiltration. When the glass was infiltrated at 1300 °C (Fig. 4(b)), the strength for the specimens C0.6 and C0.4 increased to over 500 MPa with the infiltration time and decreased after 180 min of infiltration. These decreases in the strength can be attributed to the exaggerated grain growth of the sample, which will be discussed later, with alumina particles with bimodal particle distribution [9]. The strength for sample C0.0 was much higher at 1300 °C than at 1150 °C. This result reveals that the higher infiltration temperature is more favorable for the porous alumina preform with fine particles due to the easy glass penetration at higher temperature. The sharp decrease in biaxial strength at the early infiltration time for sample C1.0, which was infiltrated at 1300 °C, is due to the swelling phenomena, which are shown in Fig. 3(b) [10–12].

3.2. Microstructure and grain growth of glass-infiltrated alumina

SEM morphologies for the glass-infiltrated alumina composites after infiltration at 1150 °C and 1300 °C for various times are shown in Fig. 5.

When the glass was infiltrated at 1150 °C (Fig. 5(a)), for the coarse sample (C1.0), the alumina grain size did not change much with infiltration time; however, the sample C0.0 showed grain growth with an increase in infiltration time. This suggests that the fine alumina particles dissolve much more easily in

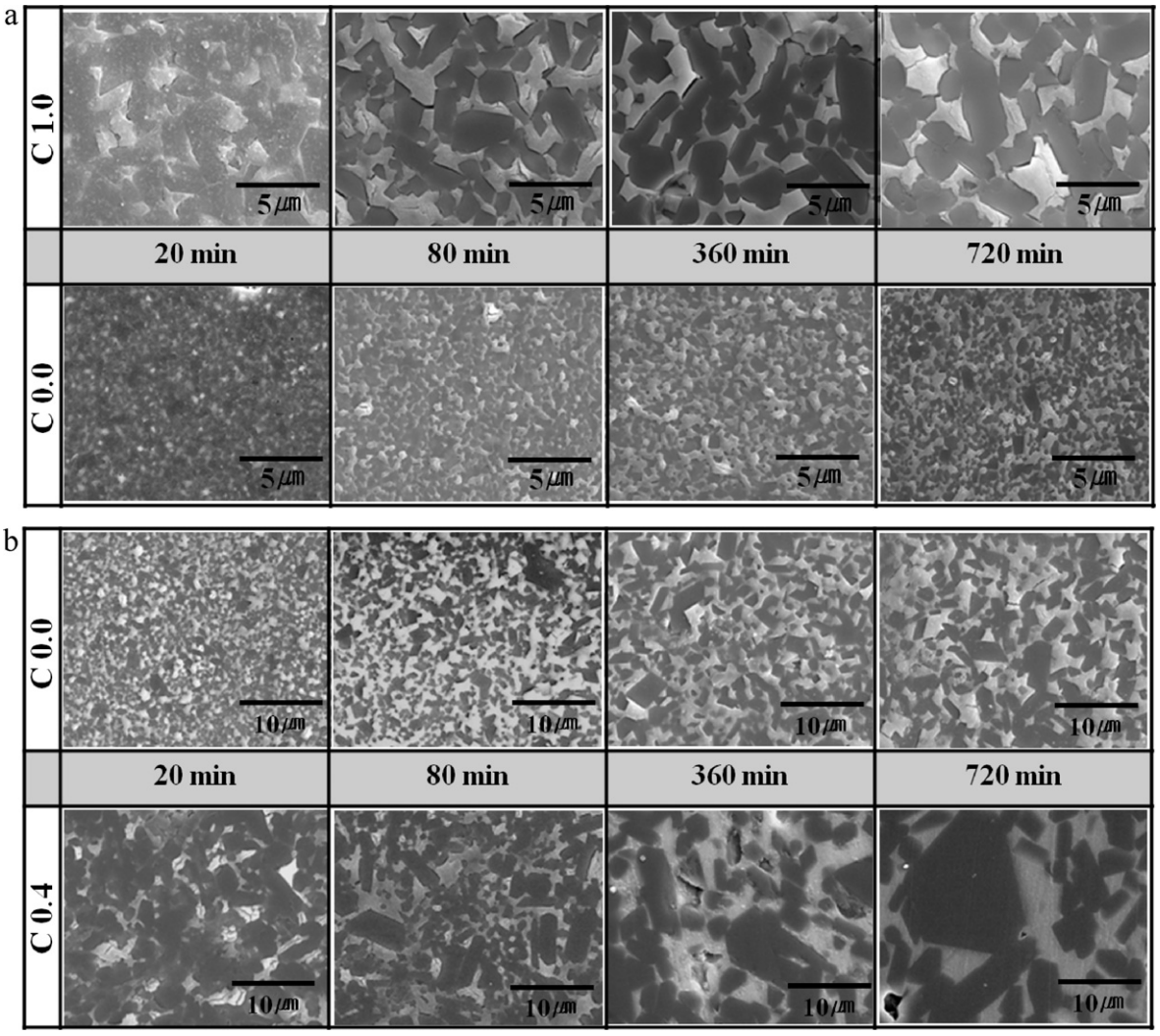

Fig. 5. SEM micrographs of the glass-infiltrated alumina after infiltration at (a) 1150 °C and (b) 1300 °C for various times (Dark: alumina, White: glass).

glass melts than coarse ones do, and that Al^{3+} and O^{2-} ions in the glass melts re-precipitate on other alumina particles to make them grow. This dissolution and re-precipitation phenomenon [13–15] can be clearly observed at higher infiltration temperatures. When the glass for the sample C0.0 was infiltrated at 1300 °C (Fig. 5(b)), tabular alumina grains in homogeneous grain growth were observed with an increase in infiltration time. The alumina grain size after 720 min of glass infiltration reached around 4.0–5.0 μm, which value is much larger than that of the sample infiltrated at 1150 °C. The lower viscosity of the glass at 1300 °C also makes the dissolution and re-precipitation easier. This observation suggests that the homogeneous grain growth and tabular shape of alumina particles result in the higher strength of the glass-infiltrated alumina [7].

For sample C0.4, which has a bimodal alumina particle distribution, however, the number of fine alumina particles continuously dropped and large alumina particles increased their sizes to make an exaggerated grain growth with the increase in filtration time. It is believed that the smaller alumina particles dissolved and that the Al^{3+} and O^{2-} ions in the glass melt re-precipitated onto the larger alumina particles [14,16]. This heterogeneous grain growth, and formation of grains with irregular shape, are a major cause of the degradation of strength [17].

TEM morphologies for the alumina grains of sample C0.0 after infiltrating at 1300 °C for 20 min and 720 min are shown in Fig. 6. Both images clearly show the crystallized tabular shape of a single crystalline alumina particle; the alumina grain size after 720 min of glass infiltration reached around 5.0 μm, which is 10 times larger than that for the sample infiltrated for 20 min.

In Ostwald ripening mechanisms [16] for grain growth during liquid phase sintering, three types of ion transfer process are described. In a contact flattening mechanism, Al^{3+} and O^{2-} ions at the contact zone of alumina particles transport to the curved zone through molten glass. In solid neck growth, these ions diffuse through grain boundaries. Both mechanisms show fixed grain size and grain density. In the third mechanism, however, the glass dissolves the fine grains and precipitates onto the larger grains. This leads to grain coarsening and reduces grain density. In the present study, the glass melt first

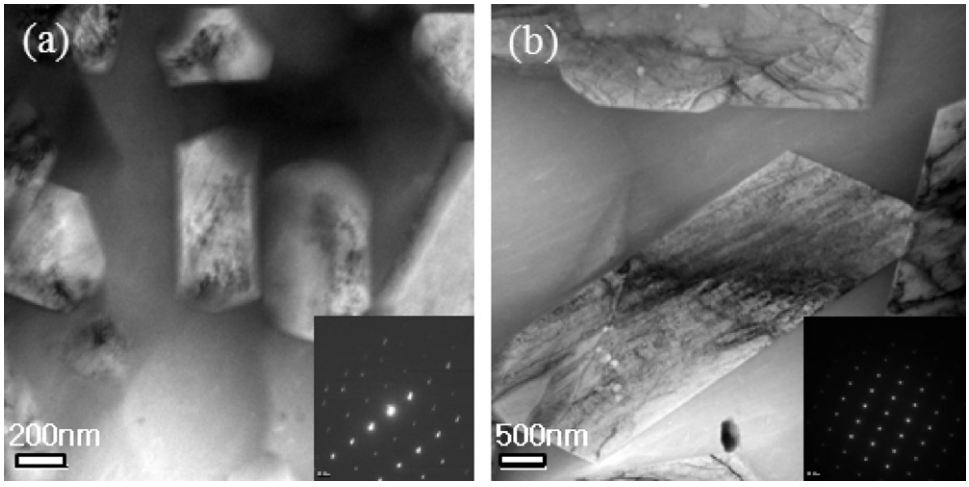

Fig. 6. TEM images of the alumina grains for the C0.0 sample after infiltrating at 1300 °C for (a) 20 min and (b) 720 min.

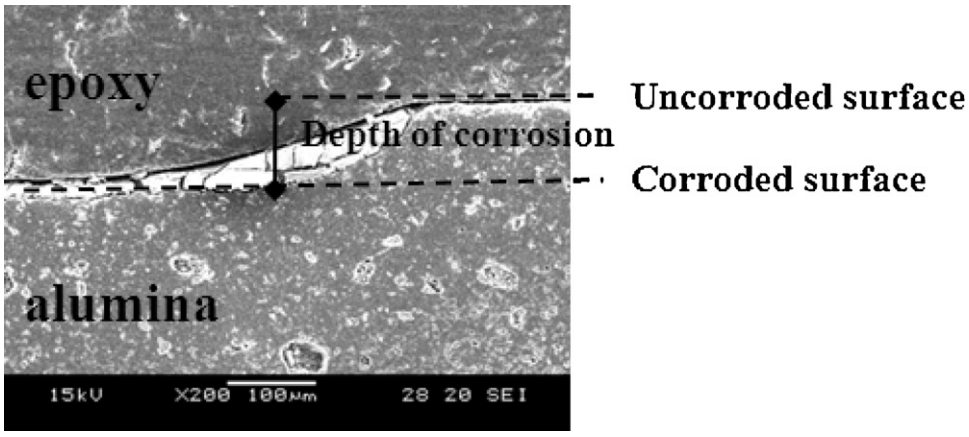

Fig. 7. SEM micrograph of cross-section of alumina disk after firing at 1300 °C for 180 min.

dissolves the finer alumina particles and precipitates onto the larger alumina particles to make them grow. The corrosion of alumina particles by glass phase affects the microstructure and strength of the composites.

3.3. Glass corrosion behavior of alumina with infiltration time

To study the glass corrosion behavior of alumina ceramics, the glass powder was placed on a sintered alumina disk and fired at 1300 °C for various times from 20 min to 360 min. The depth of corrosion was measured from SEM images for the cross-section of the sample, as shown in Fig. 7. After dissolving the specimens with 50 vol%-HF solution for 2 weeks, the weight loss was also measured in order to calculate the amount of alumina corroded into the glass from the sintered alumina disk. It is known that only silicate glass, not alumina, can be dissolved easily in HF solution. Fig. 8 shows the depth of corrosion and the amount of alumina corroded from the sintered alumina disk after corrosion at 1300 °C for various times.

The corroded depth was increased within the 180 min of corrosion time, and stayed constant after that. The glass corrosion for the alumina disk stopped after a certain firing time and the maximum depth of corrosion was 110 μm. At this point the increased concentration of Al^{3+} ions in the glass melt prevented the further corrosion of alumina because the concentration gradient between the alumina and the glass melt became smaller. The amount of alumina corroded, however, increased up to 180 min of corrosion time and decreased

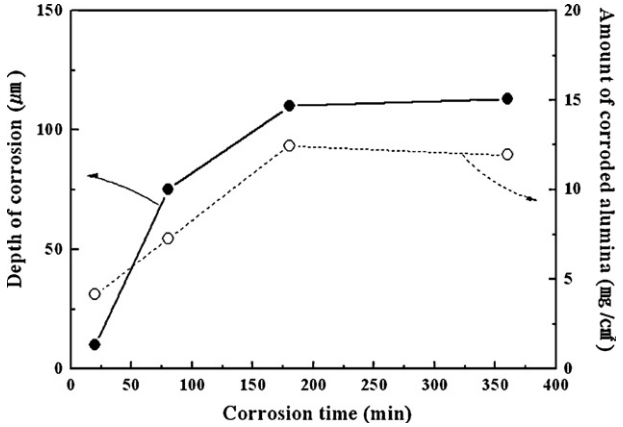

Fig. 8. Depth of corrosion and amount of sintered alumina after corrosion at 1300 °C for various times.

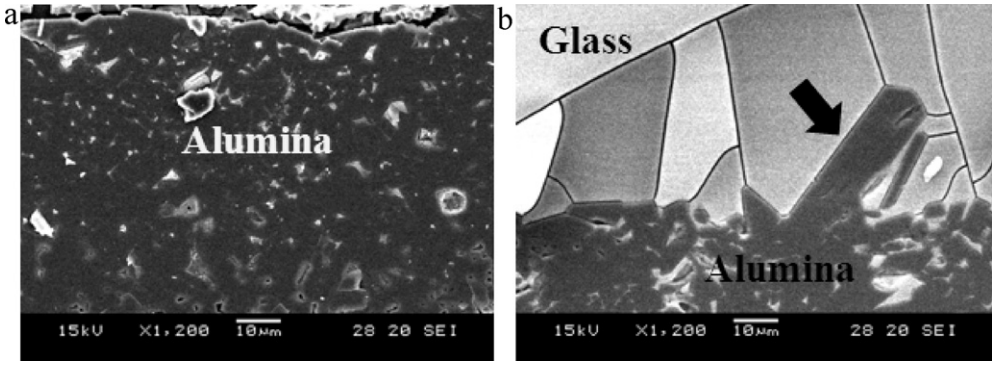

Fig. 9. SEM micrographs of the cross-section of alumina disk after firing at 1300 °C for (a) 20 min and (b) 360 min.

slightly after that. This suggests that the Al^{3+} and O^{2-} ions in the glass melt re-precipitated on the alumina surface.

Fig. 9 shows the SEM images for the interface between the glass and the alumina after firing at 1300 °C for 20 min and 360 min. A tabular shape of the alumina grains was observed when the sample was fired for 360 min as shown in Fig. 9(b). It is believed that, as shown in Fig. 5, the Al^{3+} and O^{2-} ions in the glass melt re-precipitated on the alumina surface.

4. Conclusions

(1) The initial rapid densification was related to the pore diameter of the alumina preform and the infiltration temperature. The sample with coarse alumina particles showed higher densification at the early stage of the infiltration time.
(2) The biaxial strength sharply increased with glass infiltration due to filling of the pores. The maximum strength of 517 MPa was obtained for the sample with a combination of fine and coarse alumina particles.
(3) Exaggerated grain growth was observed in a sample that had a longer infiltration time because the glass dissolved the fine alumina grain and then the Al^{3+} and O^{2-} ions in the glass melt re-precipitated onto the larger alumina grain.

Acknowledgement

This work was supported by an INHA UNIVERSITY Research Grant.

References

[1] S. Jill Glass, D.J. Green, Permeability and infiltration of partially sintered ceramics, J. Am. Ceram. Soc. 82 (10) (1999) 2745–2752.
[2] Y.-G. Jung, I.M. Peterson, A. Pajares, B.R. Lawn, Contact damage resistance and strength degradation of glass-infiltrated alumina and spinel ceramics, J. Dent. Res. 77 (3) (1999) 804–814.
[3] R.W. Wassell, A.W.G. Walls, G. Steele, Crowns and other extra-coronal restorations: provisional restorations, Br. Dent. J. 192 (4) (2002) 199–211.
[4] D.Y. Lee, Optical, mechanical properties infiltration rate of spinel/zirconia-glass dental composites prepared by melt infiltration, J. Mater. Sci. 39 (9) (2004) 3141–3145.
[5] H. Hornberger, P.M. Marquis, Microstructure of high strength glass composite, J. Mater. Res. 11 (4) (1996) 855–858.
[6] D.Y. Lee, D.J. Kim, B.Y. Kim, Y.S. Song, Effect of alumina particle size and distribution on infiltration rate and fracture toughness of alumina-glass composites prepared by melt infiltration, Mater. Sci. Eng. A 341 (2003) 98–105.
[7] J.H. Lee, C.Y. Kim, Effect of glass composition on the properties of glass-infiltrated alumina(i): effect of Al_2O_3, J. Korean Ceram. Soc. 40 (3) (2003) 301–308.
[8] W.D. Kingery, Densification during sintering in the presence of a liquid phase: I. Theory, J. Appl. Phys. 30 (1959) 301–306.
[9] H.S. Song, R.L. Coble, Origin and growth kinetics of platelike abnormal grains in liquid-phase-sintered alumina, J. Am. Ceram. Soc. 73 (7) (1990) 2077–2085.
[10] A.P. Savitskii, N.N. Burtsev, Compact growth in liquid phase sintering, Sov. Powder Metall. Met. Ceram. 30 (1979) 488–493.
[11] I.M. Robertson, G.B. Schaffer, Swelling during liquid phase sintering of Ti–Ni alloys, Powder Metall. 52 (3) (2009) 213–224.
[12] A.P. Savitskii, N.N. Burtsev, Volume changes experienced by Al–Zn compacts during liquid-phase sintering, Sov. Powder Metall. Met. Ceram. 21 (1982) 760–764.
[13] F.V. Lenel, Sintering in the presence of a liquid phase, Trans. AIME 175 (1948) 878–905.
[14] T.Y. Chan, S.J. Lou, S.T. Lin, Effects of high concentrations of liquid phase and magnesia on the grain growth of alumina, Ceram. Int. 24 (1998) 617–625.
[15] B. Meredith, D.R. Milner, Densification mechanisms in the tungsten carbide cobalt system, Powder Met. 19 (1976) 162–170.
[16] S.S. Kang, S.T. Ann, D.N. Yoon, Determination of spherical grain size from the average area of intersection in Ostwald ripening, Metallography 14 (1981) 267–270.
[17] M. Schreiner, B. Lux, On the origin of discontinuous grain growth during – liquid phase sintering of WC – Co cemented carbides, Powder Met. Inter. 16 (1984) 180–183.